Renewable Energy 77 (2015) 338–350

Contents lists available at ScienceDirect

Renewable Energy

journal homepage: www.elsevier.com/locate/renene

Blade loading on tidal turbines for uniform unsteady flow

I.A. Milne [a, *], A.H. Day [b], R.N. Sharma [a], R.G.J. Flay [a]

[a] Department of Mechanical Engineering, The University of Auckland, Private Bag 92019, Auckland Mail Centre, Auckland 1142, New Zealand
[b] Department of Naval Architecture and Marine Engineering, University of Strathclyde, Henry Dyer Building, 100 Montrose Street, Glasgow G4 0LZ, UK

ARTICLE INFO

Article history:
Received 22 January 2014
Accepted 10 December 2014
Available online 30 December 2014

Keywords:
Unsteady hydrodynamics
Tidal turbine
Dynamic inflow
Added mass
Towing tank testing

ABSTRACT

An improved characterisation of the unsteady hydrodynamic loads on tidal turbine blades is necessary to enable more reliable predictions of their fatigue life and to avoid premature failures. To this end, this paper presents a set of blade-root bending moment responses for a scale-model tidal turbine subjected to an unsteady planar forcing in a towing tank. In cases where the boundary layer was believed to be attached to the outer sections of the blade, the out-of-plane bending moment amplitude for unsteady flow was up to 15% greater than the corresponding load measured in steady flow and exhibited a phase-lead of up to 4.5°. Both these observations are qualitatively consistent with the effects of dynamic inflow and non-circulatory forcing. The bending moment responses for a forcing time history that comprised multiple frequencies, as well as for a discrete half-sinusoidal perturbation, were able to be reconstructed reasonably well using the responses obtained from single-frequency oscillatory flows. This suggests that blade designers could utilise relatively low fidelity techniques and conduct potentially fewer experimental tests to acquire the fatigue load spectrum.

© 2014 Elsevier Ltd. All rights reserved.

1. Introduction

If tidal stream energy is to prove competitive with other forms of energy generation, tidal turbines must be economical to manufacture and also operate reliably over their design life of 20 years or more [9,25]. Reliability is arguably an even greater concern for turbines which are deployed in remote communities, where replacement components and expertise are not likely to be readily available and electricity supply could be jeopardised [1].

The turbulent flow which is onset to the turbine presents a significant technical challenge for designers. Failures of early generation tidal turbines have been cited to be a consequence of a poor understanding of the magnitudes and the spectral characteristics of the resulting hydrodynamic loads [13]. Compounding the issue is that questionable assumptions and safety factors are widely used in predicting the unsteady loads of tidal turbine blades [9,26].

This can be attributed, in part, to a lack of experimental data on the unsteady hydrodynamic loading on tidal turbines for a forcing that is representative of the unsteady flow. This data is necessary to understand the underlying phenomena which are present, to quantify the loading and subsequently, to ascertain the level of complexity that is required for modelling the loads and predicting fatigue life.

It is important to also consider that similar issues are faced by designers of hydro-kinetic turbines which are deployed in rivers and canals [10]. Therefore, providing an improved characterisation of the unsteady blade loads is expected to draw wide interest.

2. Literature review

2.1. Unsteady loading of rotors

The unsteady hydrodynamic loads of a rotor that is subjected to an axial flow perturbation include both circulatory and non-circulatory components. Provided that the boundary layer remains attached to the foil at the outer sections of the blade, the unsteady circulatory forces are attributed to the vorticity that is shed from the blade and then trailed in the wake. For perturbations with frequencies relatively small in comparison to the rotational frequency of the rotor, the circulatory loading is commonly associated with dynamic inflow. These circulatory effects were first observed for helicopter rotors in the 1960s and have been discussed by researchers such as [17] and [12].

The dynamic inflow phenomenon can be attributed to the induced flow in the trailed wake taking time to reach a new equilibrium state

* Corresponding author. Tel.: +64 9 373 7599; fax: +64 9 373 7479.
E-mail addresses: imil015@aucklanduni.ac.nz (I.A. Milne), sandy.day@strath.ac.uk (A.H. Day), r.sharma@auckland.ac.nz (R.N. Sharma), r.flay@auckland.ac.nz (R.G.J. Flay).

http://dx.doi.org/10.1016/j.renene.2014.12.028
0960-1481/© 2014 Elsevier Ltd. All rights reserved.

Nomenclature

λ	tip-speed ratio, $\Omega R/U$
μ	current number, $\tilde{u}/U$
Ω	rotational speed of rotor (rad s^{-1})
$\tilde{u}$	maximum oscillatory carriage velocity (m s^{-1})
A	swept area of rotor (m^2)
C_M	blade-root bending moment coefficient for steady-flow, $M/\frac{1}{2}\rho U^2 AR$
C_P	power coefficient, $P/\frac{1}{2}\rho U^3 A$
C_T	thrust coefficient, $F_x/1/2\rho U^2 A$
f	oscillatory frequency of carriage (Hz)
F_x	axial (thrust) force on rotor shaft (N)
k	reduced frequency, $\pi cf/\Omega r$
k_{M_y}	out-of-plane blade-root bending moment coefficient normalised by the tip-speed, $M_y/\frac{1}{2}\rho(\Omega R)^2 AR$
m	frequency ratio, $2\pi f/\Omega$
M_x	blade-root in-plane bending moment (N m)
M_y	blade-root out-of-plane (thrust-wise) bending moment (N m)
n_s	sampling frequency (Hz)
R	radius of rotor tip from hub centre (m)
U	steady carriage speed (m s^{-1})
M_{yQS}	blade-root out-of-plane bending moment measured in steady-flow at the equivalent instantaneous velocity and rotor speed (N m)
$\overline{M_{y_{QS}}}$	blade-root out-of-plane bending moment measured in steady-flow at the mean tip-speed ratio (N m)

following a change in loading at the rotor plane. The lag in the induced velocity response effectively gives rise to a phase-lead in the incident velocity at the blade section relative to the axial velocity in the free-stream [23]. This subsequently also results in a phase-lead and overshoot in the bending moment response of the blades, relative to the quasi-steady loading.

The non-circulatory loads arise due to the pressure forces which are required to accelerate the fluid in the vicinity of the blade [11]. This forcing is independent of the presence of the rotor wake and acts 180° out-of-phase with acceleration. For a perturbation in the axial velocity, this implies that the non-circulatory forcing also gives rise to a phase-lead in the loading over the velocity.

Whilst the unsteady loads of wind turbines subject to an axial forcing have been investigated and found to be relatively small [20], they have been seldom reported for tidal turbines. In fact, [23] argued that the effects of an axial velocity perturbation may be comparatively more significant for tidal turbines than for helicopter rotors or wind turbines. This is owing to the ratio of the fluid to structural density being much closer to 1 than for rotors in air. This reinforces the need to quantify its contribution.

2.2. Experimental investigations of unsteady tidal turbine loading at model-scale

A variety of techniques have been employed to study the unsteady loading of horizontal-axis tidal turbines in the laboratory. Ref. [14] acquired measurements of the mean thrust on the tower structure of a 700 mm diameter (approximately 1/30th scale) tidal-turbine in a flume, where the turbulence intensity in the flow was varied from 8% to 25%. However, the spectral characteristics of the turbulence were not reported, and it is difficult to relate these results to a full-scale turbine. Furthermore, the perturbations in the thrust were not reported and it cannot be ascertained whether any overshoots in the loading were present.

Ref. [3] reported on experiments of a model tidal turbine towed at constant velocity in a still-water tank, where the unsteady flow was instead imparted from surface waves. Unlike other wave-based experiments, such as those of [8]; the blade-root bending moment was specifically measured. Acquiring the bending moment response from individual blades is deemed to be more suitable for quantifying the unsteady loading. This is because the non-coherent loading imparted by the surface waves would not be uniform over all three blades and could therefore only be determined in an averaged sense from thrust measurements from the shaft or support structure. Furthermore, additional losses through the shaft bearings etc. do not have to be accounted for if blade root bending moments are measured directly.

For relatively low frequency and small amplitude surface waves, Ref. [3] found that the bending moment response compared reasonably well with a prediction using a quasi-steady numerical blade element-momentum model with no acceleration effects included. This implies that the unsteady hydrodynamic contribution for these cases was relatively small. However, establishing the contribution from the non-circulatory and circulatory forcing is difficult, owing to the need to estimate the kinematics of the flow using measurements of the water surface elevation in conjunction with a linear wave theory. Additionally, inferring relatively small phase differences from measurements of the free surface to quantify the unsteady loading is particularly challenging.

The study by Ref. [23] involved perturbing a 300 (mm) diameter twin-bladed rotor using a towing carriage. These experiments were conducted in a flume with a steady flow and the total axial thrust was inferred from the force applied to the fixed structure that supported the rotor. It was the first investigation that attempted to establish the relative contribution of the forcing components in-phase and out-of-phase with velocity of a tidal turbine. However, as the quasi-steady loading would also appear in-phase with velocity and was not removed, quantifying the unsteady hydrodynamic contribution alone from these results is inherently complicated.

Whilst the investigation by Ref. [23] showed promise, the experimental set-up was subject to not only the challenges of speed control, high blockage and background unsteadiness, but also to the presence of a low frequency wave. These issues restricted the maximum oscillatory frequency that was able to be investigated to approximately $f = 0.1$ Hz. This corresponded to a reduced frequency limit at the radial location of $r = 0.75R$, where R is the rotor radius, of approximately $k = \pi fc/\Omega r = 0.02$, where c is the local chord and Ω is the rotational speed of the rotor. As discussed by Ref. [15]; these reduced frequencies are up to 6 times smaller than could be imparted by turbulence due to the effect of rotational sampling and are considered to be representative of large eddies. Therefore, it is possible that the effects of unsteadiness on the loads were inherently small at these relatively low frequencies.

In an attempt to overcome some of these shortcomings, the investigation of Ref. [16] adopted the approach of superimposing an unsteady surging motion upon a steady forward speed in calm water in a towing tank. A tri-bladed turbine was used in the study, where the blockage was relatively low at approximately 5%, the rotor speed was maintained constant and the blade-root bending moments were measured. The study demonstrated that for a turbine perturbed about a tip-speed ratio near maximum power, the unsteady bending moments can be significant and 25% greater than the maximum load under steady flow. However, these large loads, which were also non-linear, were believed to be affected by separation of the boundary layer on the foil and dynamic stall. This complicated the identification and quantification of the contribution to the loads from the unsteady attached flow phenomena.

The measurements of Ref. [16] also indicated that at higher tip-speed ratios, where no dynamic stall was believed to be present at the outer blade sections, the response tended to be comparatively more linear. Therefore, conducting the experiments at similarly high tip-speed ratios was deemed to be more suitable for quantifying the relative contribution of the dynamic inflow (circulatory) and non-circulatory forcing to the loading in terms of an amplitude and phase, and allowing the construction of a relationship akin to a transfer function. It is also important to consider that higher tip-speed ratios conditions may also be of more interest for tidal turbines which employ active pitch control for power regulation and are less likely to experience dynamic stall.

The aforementioned studies have also generally been restricted to single frequency oscillatory motion. However, Ref. [16] briefly demonstrated that their experimental-set up could be employed to generate a more general forcing, comprising multiple oscillatory frequencies. Therefore, the methodology is also attractive for investigating the applicability of using a linear superposition of the single frequency responses to synthesise the response to a multi-frequency forcing and to large eddies. Such approaches may potentially offer blade designers with a relatively simple approach to acquire the preliminary fatigue loads of a turbine.

3. Objectives

The primary objective of the present study was to quantify experimentally the unsteady loads on a horizontal-axis tidal turbine blade from a forcing that was representative of onset turbulence and for operating conditions where the boundary layer remained primarily attached to the foil.

In meeting this objective, the intention was to obtain a new, more comprehensive dataset of the bending moment response to oscillatory frequency and velocity amplitude, and corresponding to a higher tip-speed ratio than reported by Ref. [16]. A subsequent aim was to perform a series of multi-frequency and discrete half-sinusoidal experiments to demonstrate whether the single frequency forcing could be applied to model these more general responses.

4. Experimental methodology

4.1. Configuration of the towing carriages & turbine design

The turbine experiments were conducted at the Kelvin Hydrodynamic Laboratory at the University of Strathclyde in Glasgow. The still water tank has a working length of 76 m, width of 4.6 m and the water level was maintained at 2.00 m. The facility is shown in Fig. 1, together with a schematic depicting the principal dimensions.

The experimental methodology and turbine was consistent with that described by Ref. [16]. A combination of two towing carriages was used to generate the unsteady forcing. The main carriage speed was held constant during the tests and replicated a mean flow past the turbine. An auxiliary carriage attached to the main carriage generated a planar perturbation driven by a computer controlled Parker ETB 100 linear actuator. The towing carriages are shown in Fig. 2 and a schematic diagram of the test set-up is provided in Fig. 3.

A horizontal-axis, tri-bladed turbine with a diameter of 780 mm and a 120 mm diameter hub was employed in the experiments and is shown in Fig. 4. This was mounted rigidly to the auxiliary carriage from above, with the rotor axis being 0.67 m below the mean free water surface. As detailed by Ref. [16]; the blades had a non-uniform profile, with the chord and twist varying along the span. The blade sections conformed to the 24% thick (defined with respect to the chord), laminar-flow NREL S814. The profile was specifically designed for the root section of small wind turbines [21]. Given this, it was deemed to provide a sufficient degree of rigidity such that hydro-elastic effects on the blades of the model tidal turbine could be neglected. Negligible elastic deformation of the blades when loaded was confirmed during initial trials.

4.2. Measurement of the blade-root bending moment

The three blades were instrumented with strain gauges in a Wheatstone bridge configuration at the blade root. These were sealed water-tight and enclosed within the rotor hub cone at a radius of $r_{sg} = 36$ mm from the rotor axis. One blade was used to

Fig. 1. Towing tank facility (above) and a schematic with principal dimensions (below).

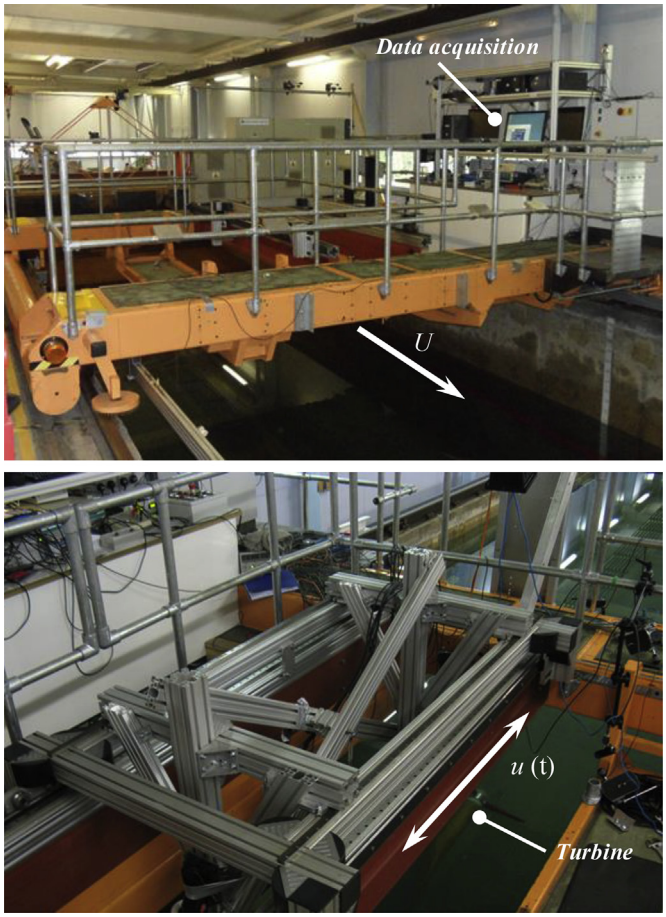

Fig. 2. Main towing carriage (above) and the auxiliary carriage with turbine installed (below).

measure the in-plane bending moment, which is defined about an axis parallel to the rotor axis. A second blade was used to measure the out-of-plane moment, which is defined about an axis perpendicular to the rotor axis, such that it is dominated by the thrust force. The measurements from the strain gauge on the third blade were not acquired due to the limited number of channels available on the slip-ring but ensured that the hub was balanced and provided a degree of redundancy.

Amplification of the strain gauge signals (and of the thrust and torque) was performed after the slip-ring, using a six channel Ogawa Seiki DSA100 strain amplifier. It is acknowledged that the slip-rings could have potentially added resistance and noise to the un-amplified signals. Upon recommendations by the slip-ring manufacturer, these effects were deemed to be minor and, assuming that the noise was Gaussian with zero mean, could be filtered out. A high signal quality was confirmed in the preliminary tests which were performed in situ, in and out of the tank.

4.3. Control strategy & achievable Reynolds numbers

The tests were performed at constant rotational speed, using a closed-loop digital controller. An EM200 DC servo system, with tacho-generator feedback, was used to provide bi-directional positional control. A Cambridge Electronic Design Power1401 data acquisition system was used to acquire all signals except the velocity of the main carriage. The sampling rate was $n_s = 376$ Hz and a low-pass digital filter with a cut-off frequency of 300 Hz was applied to all signals in real time.

The use of a tachometer in the speed control loop and a limitation on the maximum voltage output of 10 V, effectively restricted the maximum rotor speed to 96 rpm. The maximum carriage velocity was also limited to approximately 1.0 m s^{-1}. This was due to the need to prevent water spilling into the turbine enclosure and to avoid overloading the torque transducer.

It was not practical to replicate the full-scale Reynolds numbers at model-scale. A rotor speed of 96 rpm corresponded to a Reynolds number at $0.75R$ of 1.05×10^5. Therefore, the model scale Reynolds numbers were an order of magnitude lower than would be expected on a full-scale turbine with a chord of the order of 1 m at a span of $0.75R$ [23]. Insights into the effects on the foil performance can be gathered from the wind tunnel tests of the 22% thick NREL S823 and the 24% laminar flow foils reported by Refs. [19] and [15]. These have shown that at these lower Reynolds numbers, whilst the lift coefficient still increases linearly proportionally with the angle of attack, its magnitude can be expected to be approximately 10% lower and the drag several orders of magnitudes greater relative to full-scale. Furthermore, pressure measurements presented by Ref. [15] revealed at low angles of attack the flow can separate from the pressure (lower) surface due to the large thickness of the foil. This results in an increase in both the lift and drag.

However, provided the lift slope is approximately linear and stable and the tip-speed ratio is not too high (to cause separation from the pressure surface), conducting experiments at lower Reynolds number are still expected to provide useful insights into the unsteady phenomenon expected on a full-scale turbine. Furthermore, a Reynolds number sensitivity emphasises that constant rotor speed control is most desirable for conducting the experiments, given that the Reynolds number would remain approximately constant during the oscillation.

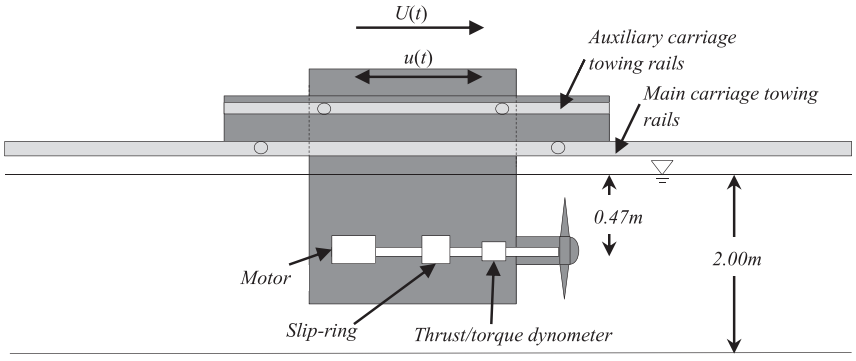

Fig. 3. Schematic diagram of the set-up for an unsteady axial forcing test.

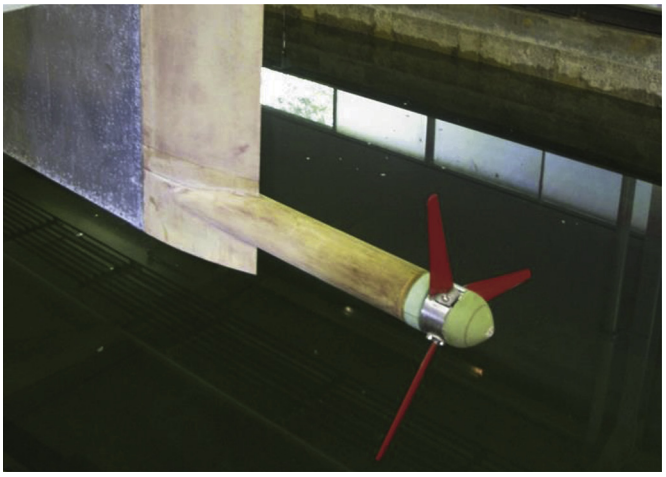

Fig. 4. Model tidal turbine prior to installation on the auxiliary carriage.

4.4. Uncertainties

The random and systematic errors inherent with the experiment were established by following the methodology of [6]. A comprehensive analysis of the experimental uncertainties is presented by Ref. [15].

For the bending moment, the random errors were smaller than the systematic errors, but were significant and implied that the total uncertainty was approximately 0.3% of the measurement. The random and systematic errors of the auxiliary carriage velocity were both dominant and the total uncertainty equated to approximately 1% of the measurement.

The random uncertainty in the rotor speed was comparatively more significant than for the steady case. However, the total uncertainty in the rotor speed was still relatively small and equal to only 0.07% of the nominal rotor speed. The uncertainties in the bending moment, velocity and rotor speeds were all considered to be adequately small for the purposes of the investigation.

5. Steady flow experiments

The power and loads of the rotor in steady flow were characterised from a series of tests which were performed at constant carriage speeds of between $U = 0.45$ m s^{-1} and 1.01 m s^{-1}, and at a fixed rotor speed of 96 rpm. This rotor speed was equivalent to that used in the unsteady tests, which facilitated a quantification of the relative unsteady contribution with minimal effects from the Reynolds number.

The coefficients of the power ($C_P = P/0.5\rho AU^3$, where ρ is the water density and A is the swept area of the rotor), thrust ($C_T = F_x/0.5\rho AU^2$) and the blade-root bending moment response ($C_{Mi} = M/0.5\rho AU^2R$, where $i = x$ for in-plane loading or y for out-of-plane loading) in steady flow are presented as a function of the tip-speed ratio ($\lambda = \Omega R/U$) in Fig. 5. It should be noted that no blockage correction was applied. For the turbine used by Ref. [2]; where the blockage in the towing tank was 8%, the thrust was estimated as being 5% greater than for unblocked conditions. Therefore, given the blockage was lower for the present tests, its effects on the loads are expected to be relatively small.

The maximum power coefficient of $C_P = 0.35$ achieved in the present tests corresponded to a tip-speed ratio of approximately $\lambda = 4$ and the power was generated by the rotor at tip-speed ratios ranging between approximately $\lambda = 2.5$ and 6.5. The maximum power is 8% lower than reported for the same turbine by Ref. [16]. This is attributed to a small blade pitch angle difference of approximately 0.5° between the two sets of experiments and the effects of the relatively low Reynolds number at the blade sections at which the experiments were conducted. In an attempt to illustrate this, wind tunnel experiments of the S814 foil presented by

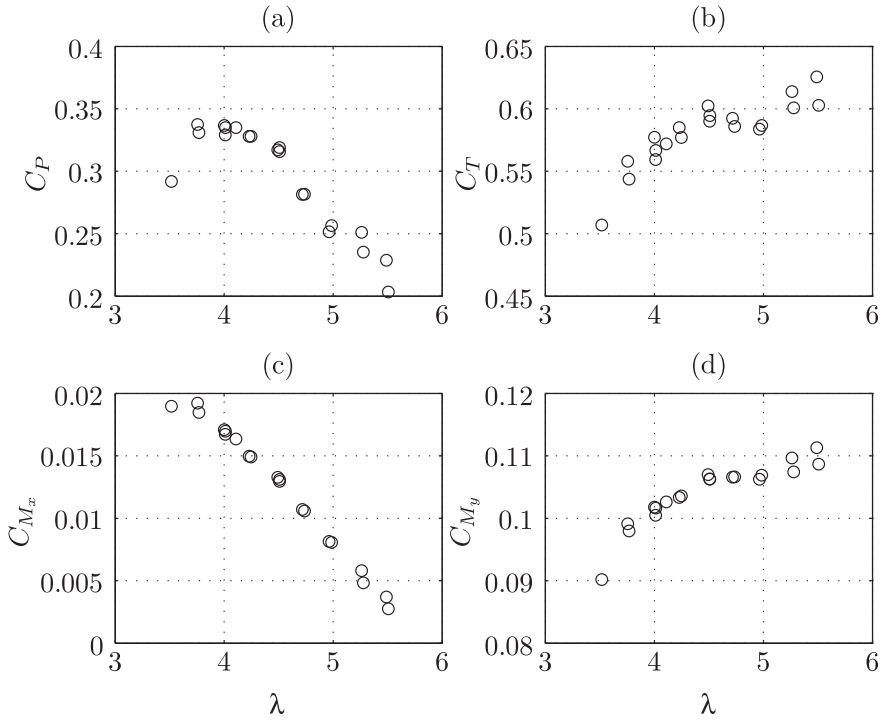

Fig. 5. Coefficients of the rotor power (a), thrust (b), in-plane bending moment (c) and out-of-plane bending moment (d) as a function of the tip-speed ratio for steady flow and at a rotor speed of 96 rpm.

Ref. [15] showed that at the Reynolds numbers used in the towing tank tests, the lift and drag coefficients at the representative angle of attack of $\alpha = 8^\circ$ were approximately $C_l = 1.12$ and $C_d = 0.066$, respectively. These values were $C_l = 1.08$ and $C_d = 0.062$ for $\alpha = 7.5^\circ$. For small angles of attack and twist and at the equivalent rotor and flow speeds, differences in the power arise through the relationship $C_l\alpha - C_d$. For $\alpha = 8^\circ$, $C_l\alpha - C_d = 0.09$ and for $\alpha = 7.5^\circ$ it is equal to 0.08, which is a difference of the order of 8%. Therefore, this is consistent with the measured reduction in the power. The sensitivity of the power also emphasises the importance of accurately setting the blade pitch for model scale testing of tidal turbines.

It can be noted that at tip-speed ratios of $\lambda < 3$ and $\lambda > 5$ the coefficients of the power, thrust and blade-root bending moments exhibit a comparatively large degree of scatter. At the very low tip-speed ratios the effects of flow separation on the suction surface of the foil are believed to begin to dominate. Conversely at relatively high tip-speed ratios, in line with the effects of the low Reynolds number discussed in Section 4.3, it is postulated that the boundary layer on the pressure surface may be relatively weak and susceptible to premature separation. At these operating states relatively small changes in the flow state can cause relatively large differences in the hydrodynamic lift and drag performance of the foil and consequently the data are less repeatable.

The magnitude of the out-of-plane blade-root bending moment coefficient is approximately 5 times larger than the coefficient of the in-plane blade-root bending moment. This is consistent with the expectation that the thrust forces, which give rise to the out-of-plane blade-root bending moment, dominate over the hydrostatic and centrifugal inertial forces [7].

The out-of-plane blade-root bending moment coefficient normalised by the rotor speed, instead of the axial velocity, i.e. $K_{M_y} = M_y/(0.5\rho(\Omega R)^2 AR)$ is presented as a function of the inverse of the tip-speed ratio in Fig. 6. The out-of-plane blade-root bending moment is shown to exhibit an approximately linear relationship with velocity between $1/\lambda = 0.20$ and 0.28 (equivalent to tip-speed ratios ranging between $\lambda = 3.5$ and 5.0 respectively). These characteristics are consistent with an approximately linear lift slope and a boundary layer that was predominantly attached to the outer blade sections [5].

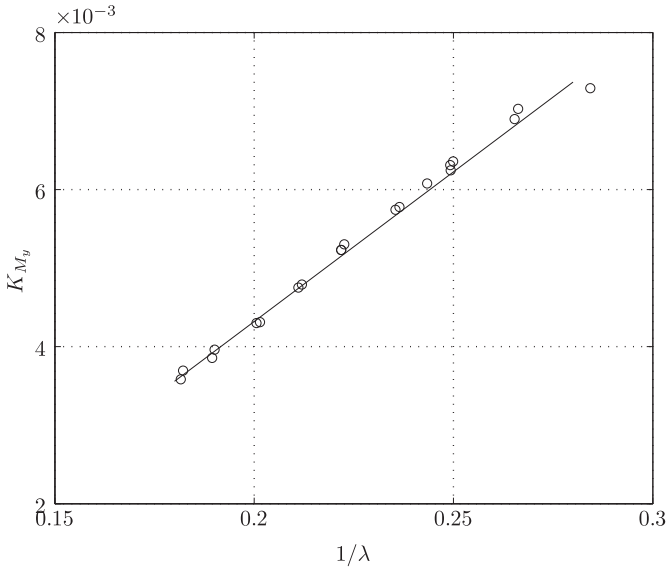

Fig. 6. Coefficients of the out-of-plane bending moment normalised by the rotor speed, as a function of the inverse of the tip-speed ratio for steady flow and at a rotor speed of 96 rpm. A linear best fit curve is superimposed on the data.

6. Single frequency oscillatory experiments

6.1. Parameter selection

The majority of the unsteady forcing experiments were performed at a mean tip-speed ratio of $\lambda = 4.5$ and a rotor speed of $\Omega = 96$ rpm. This was intended to ensure that the turbine operated within the range of states where near linearity in the loading with velocity could be expected under steady conditions, as indicated by the K_{M_y} versus $1/\lambda$ response. It was also considered to be an appropriate operating point for acquiring data to investigate the applicability of using linear superposition to reconstruct a multi-frequency forcing; see Section 7.1.

The oscillatory frequencies and velocity amplitudes that were investigated were an attempt to replicate the forcing that would likely be imparted by onset turbulence. The range of frequencies was generally $0.40 < f \leq 0.80$ Hz, with the maximum frequency being restricted by the technical limitations with the controller. These values correspond to reduced frequencies at a section at $0.75R$ of up to $k \leq 0.05$. For a typical full-scale tidal turbine, this corresponds to a turbulent eddy wavelength of 10 m. It is approximately 50% of the maximum reduced frequency likely to be expected for a tidal turbine, due to rotational sampled turbulence [15]. Despite this, these frequencies were significantly greater than those which have been reported at $0.75R$ for tidal turbines by Ref. [23]. Higher reduced frequencies were also possible for specific cases where the velocity amplitude was relatively large.

The velocity amplitude ($\tilde{u}$) was scaled using the Current number $\mu = \tilde{u}/U$, which may be considered to be a parameter analogous to the turbulence intensity. The Current number was required to be at least $\mu = 0.010$ for a single frequency oscillation, and $\mu = 0.075$ when combined in a multi-frequency test. This ensured that the motion generated by the actuator was of sufficiently good quality for fitting a linear model to the forcing. The present study also encompassed a more comprehensive set of Current numbers than was reported by Ref. [16]. The maximum Current number of $\mu = 0.250$ replicated the amplitude which could be expected at full-scale due to onset turbulence and a non-uniform mean velocity profile [15].

6.2. Data processing

The oscillatory data analysed were obtained once the main carriage had achieved a constant velocity and after at least two oscillations had been completed to allow for the decay of non-periodic initial transients. Due to the finite length of the towing tank, the total number of oscillations that comprised each test varied with the oscillatory frequency. For the lowest frequency considered, at least 10 oscillations were possible. As detailed by Ref. [15]; a cycle-by-cycle analysis detailed showed that this was a sufficient number for inferring the hydrodynamic blade load response as the phase-averaged out-of-plane bending moment response typically converged after two oscillatory cases.

The once-per-revolution, gravitational contribution that was measured for zero carriage velocity and at a very low rotational speed of 3 rpm was subtracted from the unsteady bending moment data. A 5th-order Butterworth infinite impulse response (IIR) digital filter with a cut-off frequency of $4f$ was applied off-line to all signals co-currently. This was applied in both forward and backward directions to eliminate any phase shift.

Estimates of the amplitude and phase (analogous to added mass and damping coefficients) of the out-of-plane blade-root bending moment were obtained using a linear model of the form.

$$M(t) = \sum_{i=1}^{N} Z_i \cos(2\pi f_i t + \Phi_i), \tag{1}$$

where Z_i is the amplitude, Φ_i is the phase of the ith oscillatory frequency component relative to the velocity and N is the number of fundamental frequency components. The model was fitted to two oscillatory cycles at a time and the coefficients were averaged across all estimates.

6.3. Response to the forcing parameters

6.3.1. Oscillatory frequency

The effect of the frequency on the blade-root bending moment response for oscillations of $0.40 < f \leq 0.80$ Hz and at a fixed Current number of $\mu = 0.150$ is first demonstrated in Fig. 7. The unsteady bending moment responses are presented here as hysteresis loops, with the phase-averaged bending moment as a function of the normalised oscillatory velocity and arrows indicating the direction of the velocity perturbation phase. The bending moment has been divided by the bending moment which was measured in steady flow at the equivalent mean tip-speed ratio ($\overline{M_{y_{QS}}}$), which can be inferred from Fig. 5. This provides a quantification of the magnitude of the bending moment perturbation in response to onset turbulence. The steady loading at the equivalent velocity is also shown and provides a qualification of the relative contribution of the unsteady forcing alone.

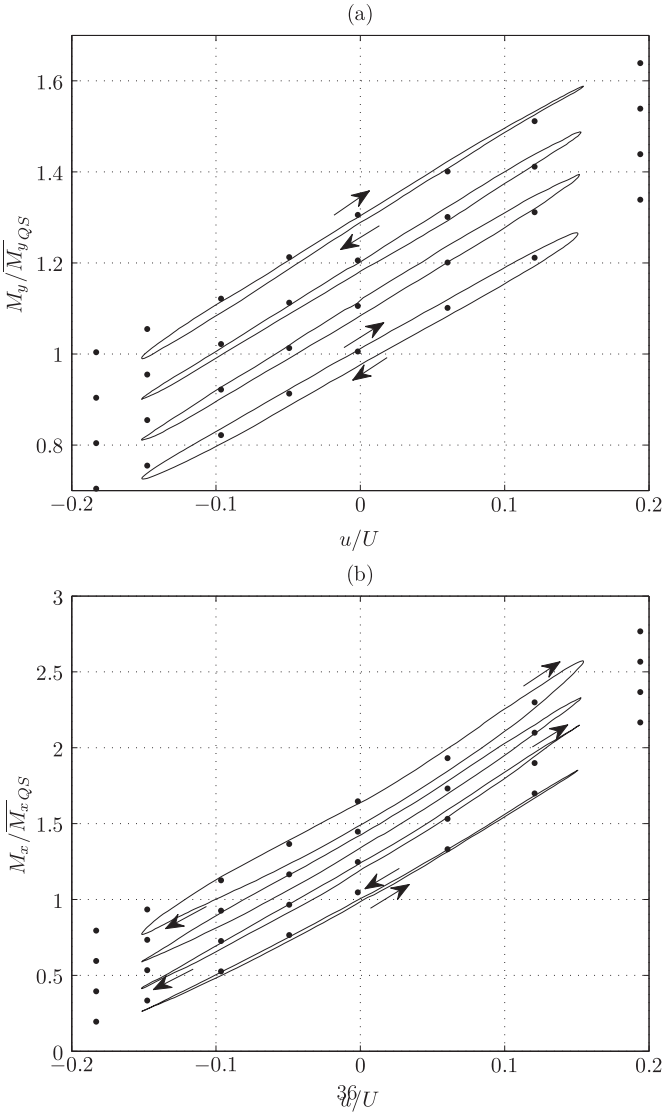

Fig. 7. Effect of the oscillatory frequency on the normalised out-of-plane (a) and in-plane (b) bending moment response for a Current number of $\mu = 0.150$. From bottom: $f = 0.40$, 0.57, 0.67 and 0.80 Hz (offset in intervals of 0.1 for clarity). The bending moments measured in steady flow at the equivalent flow speed and rotor speed are denoted by the dots. The directions of the responses relative to the phase of the velocity are depicted by the arrows.

For these frequencies the unsteady response of the out-of-plane bending moment exhibits an approximately linear relationship with velocity. Given this and based on the wind tunnel measurements of the foil presented by Ref. [15]; it is postulated that the boundary layer remains attached across the outer sections of the blades in these conditions. The loops reveal a relatively small increase in the unsteady blade-root bending moment range with the frequency (i.e. the average between increasing and decreasing axial speed phases of the loop increases); increasing from $M_y/\overline{M_{y_{QS}}} = 0.54$ at 0.40 Hz to 0.60 at 0.80 Hz.

The hysteresis loops of the out-of-plane blade-root bending moment exhibit a clockwise trajectory as indicated by the arrows. This implies a phase-lead of the unsteady bending moment over the velocity and, therefore, positive hydrodynamic added axial inertia. Both an overshoot of the steady load in the out-of-plane bending moment and a phase-lead over velocity are qualitatively consistent with the effects attributed to dynamic inflow and the non-circulatory forcing [23]. The loops become narrower and the phase-lead reduces as the frequency (and axial acceleration) is increased. A reduction in the phase-lead suggests that the induced velocity in the wake may have been less able to adapt to the changes in loading at the rotor plane at higher frequencies, tending towards a frozen-wake state.

The response of the in-plane bending moment is comparatively more non-linear than the out-of-plane bending moment. There appears to be a relatively small increase in the amplitude of the in-plane bending moment with frequency and a phase-lag over velocity is observed for all but the lowest frequency case. A phase-lag is consistent with the expectation that if there is no misalignment in the system, there should be negligible contribution to the in-plane bending moment from either the non-circulatory forcing or dynamic inflow that could otherwise impart a phase-lead.

6.3.2. Velocity amplitude

The bending moment responses to Current numbers in the range $0.100 < \mu \leq 0.250$ at an oscillatory frequency of $f = 0.40$ Hz ($k = 0.02$) are presented in Fig. 8. At this relatively low frequency, the out-of-plane bending moment remained approximately linear for all the Current numbers considered. For the out-of-plane bending moment, the magnitude of the component which appears in-phase with acceleration increases with frequency (i.e. the loops become wider). This is consistent with the non-circulatory contribution having increased with an increase in the axial acceleration. For the in-plane bending moment, the component in-phase with velocity is relatively small for all the Current numbers considered. This also concurs with notion of the in-plane loads being relatively insensitive to the non-circulatory forcing.

As demonstrated in Fig. 9, similar trends in the out-of-plane bending moment responses to an increase in Current number are observed at the higher frequencies of $f = 0.67$ Hz (solid curves) and $f = 1.00$ Hz (dashed curves). These cases also show that the non-linearities in the responses become pronounced at high Current numbers as the frequency is increased. These non-linearities give rise to a relatively large bending moment compared to the steady load. For example, for a Current number of $\mu = 0.250$, the bending moment range increased from $M_y/\overline{M_{y_{QS}}} = 0.83$ at $f = 0.40$ Hz to 0.98 at $f = 1.00$ Hz, which is an 18% increase.

The general form of the responses at these relatively high Current numbers is consistent with those reported by Ref. [16]. As the non-linearities are only present for a part of the oscillatory cycle and at high instantaneous velocity, they are primarily attributed to unsteady circulatory effects at the blade-section level. The authors are not aware of literature of the unsteady response of S814 foil at high angles of attack at the Reynolds numbers at which these data were acquired. However, these responses share qualitatively similar characteristics to the full-scale measurements of the same foil undergoing oscillations in pitch reported by Ref. [21]. In line with [12] and as discussed by Ref. [16]; it is postulated that in unsteady flow there is a delay in the boundary layer response on the foil and the movement of the trailing-edge separation point to the excitation. This could have increased the lift generated by the foil at high angles of attack relative to that expected for steady flow.

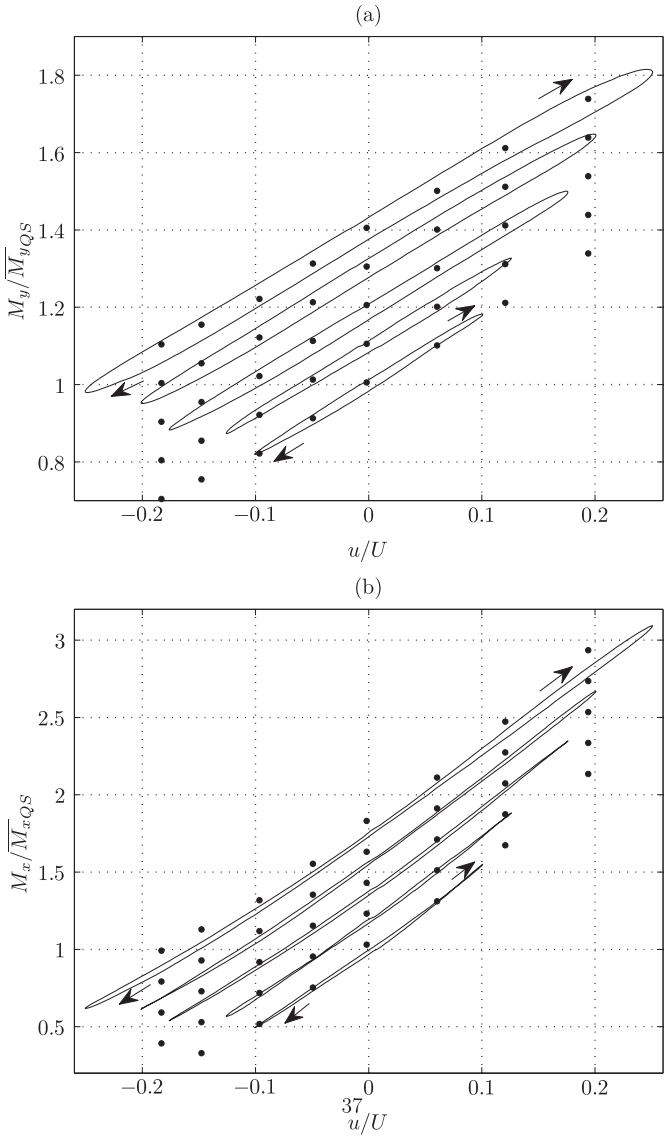

Fig. 8. Effect of the velocity amplitude on the normalised out-of-plane bending moment response for an oscillatory frequency of $f = 0.40$ Hz. The curves are consecutively offset in intervals of 0.1 from bottom, and correspond to Current numbers of $\mu = 0.100$, 0.125, 0.175, 0.200 and 0.250 respectively. The bending moments measured in steady flow at the equivalent flow speed and rotor speed are denoted by the dots.

6.4. Quantification of the unsteady contribution

6.4.1. Amplitude & phase

The estimates of the normalised amplitude and phase corresponding to the out-of-plane bending moment response for Current numbers of $0.100 < \mu \leq 0.175$ and frequency ratios ($m = 2\pi f/\Omega$) of $0.25 < m \leq 0.50$ ($0.40 < f \leq 0.80$ Hz) are presented in Fig. 10. To provide a quantification of the relative magnitude of the unsteady contribution, these amplitudes are normalised by the bending moment amplitude for steady flow. This steady flow amplitude was obtained from the linear fit that is presented in Fig. 5, where the local gradient is equal to $\delta_{M_y} = 11.9\delta U$.

The normalised amplitude increases with frequency from approximately 1.05 to 1.15, whilst the relatively small phase-lead decreases from approximately $\Phi = 4.5°$ to 1.5°. The normalised amplitudes decrease with the Current number, an effect which appears to be more significant at low frequencies. To explain the effect of the Current number, it can be noted that at relatively large amplitudes, the steady loads were more non-linear at higher instantaneous velocities, with the local gradient decreasing. As the frequency was increased, the delayed separation was expected to have increased the lift coefficient. This would have effectively increased the amplitude of the response. As such, the response would have been in closer agreement to the linear, steady flow load that was used for normalisation.

6.4.2. Relative contribution from non-circulatory forcing

The component of the bending moment that appears in-phase with acceleration contains both circulatory and non-circulatory forcing contributions. Its sensitivity to the forcing provides interesting new insights into the role of the underlying hydrodynamic phenomena. The non-circulatory forcing was estimated following [24]; whereby the blade was represented as a series of cylindrical sections for which the hydrodynamic added moment was computed as $M_{y_{nc}}(r) = 0.25\rho\pi c^2 r$ [18].

The ratio of the bending moment in-phase with acceleration to the bending moment due to the non-circulatory forcing ($M_{y_{ii}}/M_{y_{nc}}$)

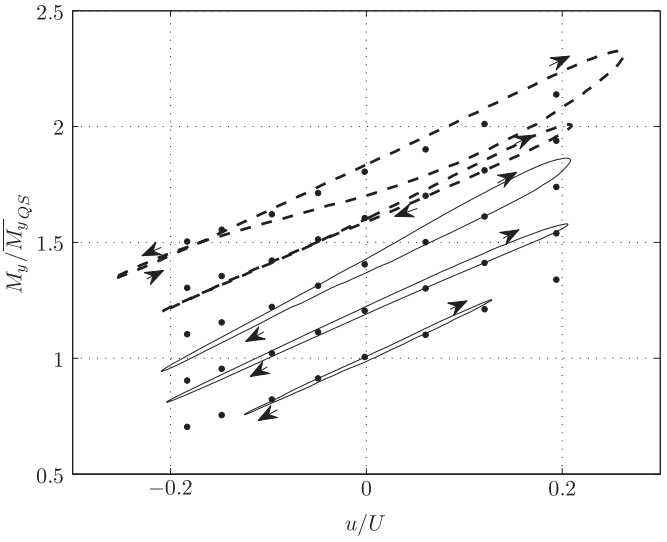

Fig. 9. Effect of the velocity amplitude on the normalised out-of-plane bending moment response for oscillatory frequencies of $f = 0.67$ Hz for Current Numbers of $\mu = 0.150$, 0.200, 0.225 respectively (solid curves) and 1.00 Hz for $\mu = 0.200$, 0.250 (dashed curves). The curves are consecutively offset in intervals of 0.1 from bottom. The bending moments measured in steady flow at the equivalent flow speed and rotor speed are denoted by the dots.

is presented as a function of the frequency ratio in Fig. 11. At low frequency ratios, the ratio $M_{y_u}/M_{y_{nc}}$ is approximately equal to 2.7 and its value decreases with frequency ratio to 0.5 for $m = 0.5$. This implies that the net circulatory forcing tends to act in opposition to the non-circulatory forcing at relatively high frequency ratios. It is also interesting to find that the coefficients are generally independent of the Current number. This suggests that the circulatory forcing is predominately a function of the frequency.

7. Applications of the single frequency oscillatory response

7.1. Multi-frequency oscillatory forcing

As previously stated, a subsequent objective of the study was to demonstrate whether the response to a more general forcing could be reconstructed using a linear superposition of the single frequency oscillatory responses. To this end, a series of multi-frequency forcing cases which comprised a superposition of the equivalent frequencies that were tested in the single frequency experiments were performed about a mean-tip speed ratio of $\lambda = 4.5$. The Current numbers for each oscillatory component were between $\mu = 0.075$ and 0.125. This was necessary to ensure that the kinematics of the forcing were sufficiently similar to the anticipated full-scale forcing and to avoid significant flow separation at the blade sections.

The bending moment response to multi-frequency forcing that comprised two relatively low frequencies of $f = 0.40$ Hz and 0.50 Hz, with a relatively low Current numbers for each component of $\mu = 0.075$ is presented in Fig. 12. To quantify the contribution from this unsteadiness, the time history is first compared with a reconstruction based on the steady loads ($\overline{M_{y_{QS}}}$) interpolated at the instantaneous velocities from the data presented in Fig. 5(d). This demonstrates that there is a relatively small overshoot of the steady load. This is in qualitative agreement with the relatively small overshoots that were observed at these frequencies for single frequency forcing, as shown in Fig. 10.

Large load cycles are of most interest for predicting the fatigue of tidal turbine blades manufactured from composite materials [22]. Given this, three relatively large load cycles have been identified in the time history. These correspond to the response between the symbols (○) and (●) respectively. The hysteresis loops corresponding to these cycles are compared with a reconstruction comprising a linear superposition of two single frequency oscillations synthesised using the equivalent amplitudes and phases that were estimated from the respective single frequency oscillatory cases presented in Fig. 10. These demonstrate that the reconstruction was able to replicate both the amplitude and phase-lead of the multi-frequency response relatively well.

A case where the forcing comprised a combination of three frequencies of 0.40 Hz, 0.50 Hz and 0.67 Hz, each with a Current number of $\mu = 0.075$ is presented in Fig. 13. As for the previous cases, the time histories demonstrate an overshoot relative to the steady loading. The hysteresis loops for four relatively large loading cycles also show that the response is able to be recovered using the amplitudes and phases of the single frequency forcing. Therefore, the cases presented in Figs. 12 and 13 provide further support for the use of the single frequency response method to model the lower frequency band of the turbulence spectrum relevant to tidal turbines.

A limitation of the use of the single frequency amplitudes and phases to reconstruct the multi-frequency response is demonstrated in Fig. 14. For this case the forcing comprised two relatively high frequency components of $f = 0.67$ Hz and $f = 0.80$ Hz and Current numbers of $\mu = 0.100$. The hysteresis loops demonstrate that through the use of a linear superposition of single frequency responses, the overshoot of the steady loads that are observed in the time history have been able to be modelled. However, the

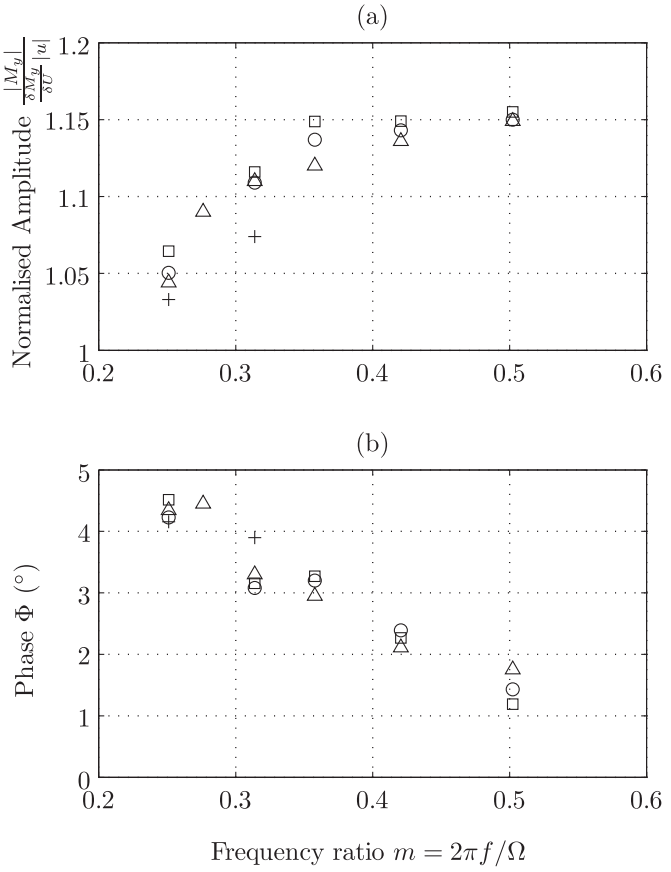

Fig. 10. Estimates of the normalised amplitude (a) and phase (b) of the out-of-plane bending moment response as a function of the frequency ratio, for Current numbers of $\mu = 0.100$ (+), 0.125 (□), 0.150 (○) and 0.175 (△).

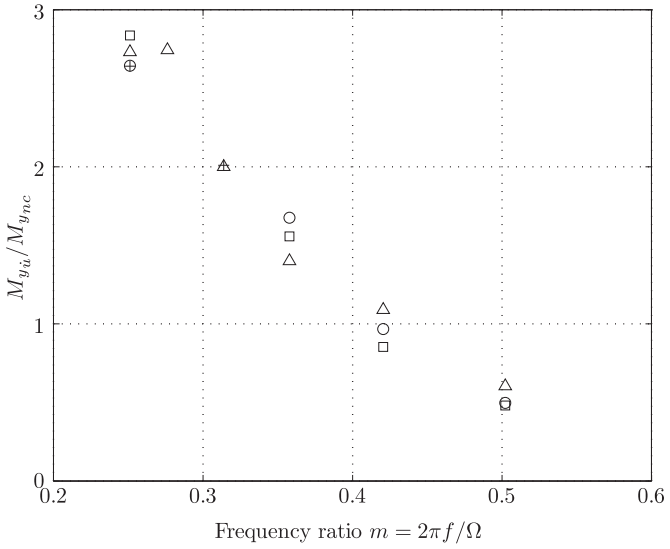

Fig. 11. Estimates of the ratio of the total out-of-plane bending moment in-phase with acceleration to that due to non-circulatory forcing alone. Data are presented as a function of the frequency ratio and for Current numbers of $\mu = 0.100$ (+), 0.125 (□), 0.150 (○) and 0.175 (△).

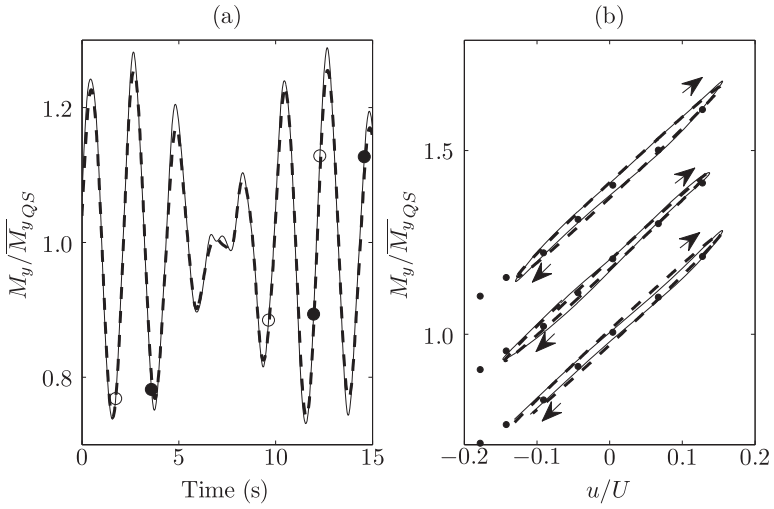

Fig. 12. Out-of-plane bending moment response to a forcing that comprised the frequencies $f = 0.40$ Hz and 0.50 Hz, each with a Current number of $\mu = 0.075$. The time history is compared with a reconstruction based on the steady forcing (dashed curve) in (a). The hysteresis loops corresponding to the time history between symbols (○) and (●) is compared with a reconstruction using a linear superposition of the individual single frequency responses (dashed curves) in (b). The bending moment measured for steady flow at the equivalent flow speed and rotor speeds is also depicted by the bullets in (b) and the hysteresis loops are offset consecutively by 0.2 for clarity.

phase-lead of the observed multi-frequency response is under-predicted.

As an independent check of the validity of linear superposition for these cases, the amplitude and phases of the individual forcing components were also estimated from the multi-frequency forcing response using the regression technique previously described in Section 6.2. These are shown in Fig. 15 for a range of test cases that were performed. The figure demonstrates that for multi-frequency forcing, the amplitudes of the individual components are approximately equivalent to the single frequency forcing functions. However, at relatively high frequencies the phase-lead is larger, similar to the responses shown in Fig. 14.

It is postulated that the circulatory forcing is the source of the larger-phase leads observed. This is because the non-circulatory forcing is expected to be linear and proportional to the acceleration. It is possible that at high frequencies the large load cycles induce circulatory transients which act to increase the phase. These would not be included in the amplitude and phases estimated for the single frequency oscillatory experiments, which were averages from multiple oscillations.

7.2. Discrete half-sinusoidal forcing

The response to isolated large eddies (analogues to gusts in the atmosphere) was investigated by subjecting the turbine to a single, half-sinusoidal motion superimposed on a steady axial velocity. These tests were physically conducted with the rotor and main carriage both at constant speeds to reduce the effect of any transients. The perturbation was created using the axillary carriage once the main carriage was positioned approximately mid-way along the length of the tank. As the intention was to also compare the response to the single frequency forcing cases, these were also performed about a mean tip-speed ratio of $\lambda = 4.5$ and a rotor speed of 96 rpm. Two relatively low frequencies of $f = 0.40$ and 0.50 Hz were considered, with a relatively large Current number of $\mu = 0.250$.

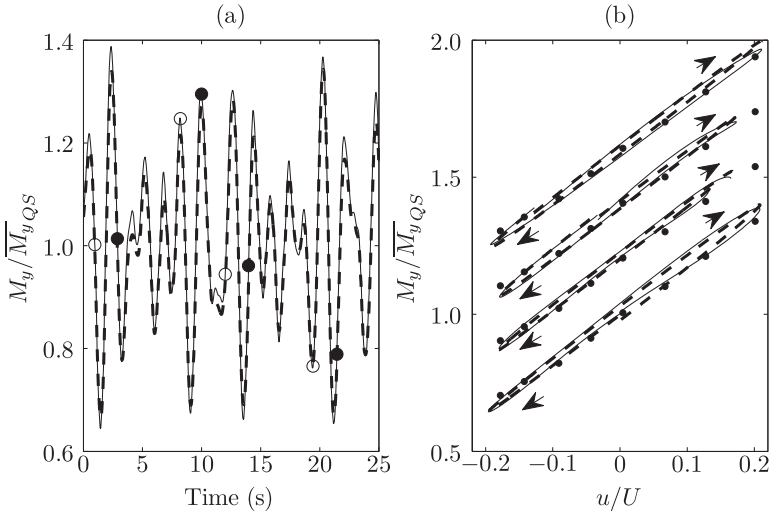

Fig. 13. Out-of-plane bending moment response to a forcing that comprised the frequencies $f = 0.40$ Hz, 0.50 Hz and 0.67 Hz, each with a Current number of $\mu = 0.075$. The presentation of the data is consistent with Fig. 12.

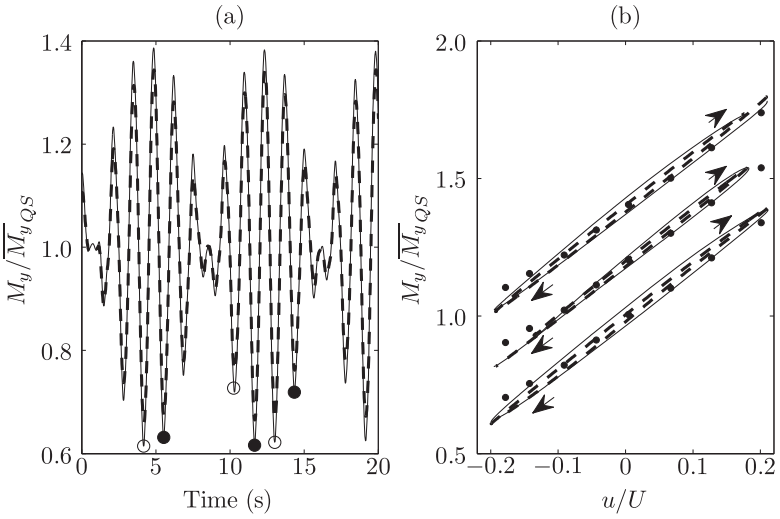

Fig. 14. Out-of-plane bending moment response to a forcing that comprised the frequencies $f = 0.67$ Hz and $f = 0.80$ Hz, each with a Current number of $\mu = 0.100$. The presentation of the data is consistent with Fig. 12.

The time histories of the out-of-plane bending moment response to a half-sinusoidal axial perturbation corresponding to these forcing parameters are presented in Fig. 16. These are first compared with a reconstruction based on the steady loads. It can be observed that there is a relatively small over-shoot of the magnitude of the steady loads for both a positive and a negative perturbation. A relatively small overshoot of the steady loads at the end of the perturbation is also identifiable. The magnitudes of the overshoots are also larger for the higher frequency case. In general, the unsteadiness decays relatively quickly after the perturbation and do not appear to be significant.

The corresponding hysteresis loops of the respective positive and negative half-sinusoidal perturbation are presented together in Fig. 17. They elucidate the phase-lead that is present in the bending moment response for each case. The oscillatory responses for the equivalent frequencies and Current number are also shown for comparison. The amplitude and the phase-lead over velocity of the discrete half-sinusoidal forcing is generally consistent with the oscillatory case. The agreement in the phase-lead implies that the combined contributions from dynamic inflow and the non-circulatory forcing are similar, despite the differences in the forcing.

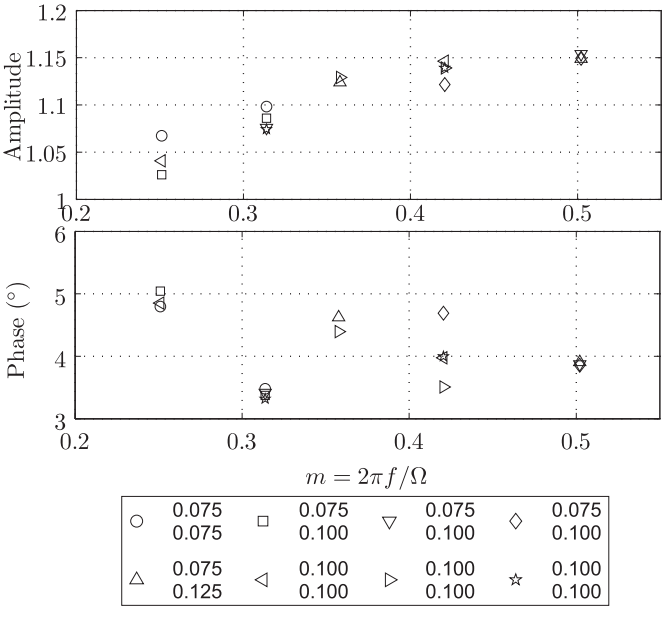

Fig. 15. Estimates of the normalised amplitude and phase of the out-of-plane bending moment response corresponding to the individual frequencies that comprised the multi-frequency forcing, acquired by fitting a bi-harmonic function to the responses. Data are presented as a function of the frequency ratio and the Current numbers of the individual frequency components are listed next to the symbol corresponding to the test case (lower frequency above).

8. Discussion

The present study has presented a more extensive set of experimental data to quantify the unsteady blade-root bending moment in attached flow than has been previously reported for tidal turbines in the literature. The finding of normalised amplitudes of up to 1.15 for single frequency oscillations (as shown in Fig. 10(a)) implies that for conditions for which the flow is considered to be predominantly attached to the blade, the maximum out-of-plane blade-root bending moment is smaller than when flow separation and stall is believed to occur; see Ref. [16]. Nevertheless, the effects of unsteady forcing in attached flow are still relatively large and are considered to require accounting for it in blade load analyses. The identification of an underlying frequency dependency in the phase of the out-of-plane bending moment is also an interesting new observation. The investigation by Ref. [23] was unable to experimentally identify any frequency dependency in the axial inertia. This may have been due to the relatively low frequencies in which those experimental data were obtained, compared to what has been achieved in this study.

There is very limited literature for other tidal turbines to compare the estimates of the amplitude and phases against. However, it is interesting to contrast the component of the bending moment that appears in-phase with the acceleration, with the hydrodynamic inertia coefficients that were reported at relatively low frequencies by Ref. [23]. These were $C_I = \{F_x\}_{\dot{u}}/\rho V\dot{u} \leq 0.05$, where $\{F_x\}_{\dot{u}}$ was the component of the axial thrust that appeared in-phase with acceleration and V was the volume enclosed by the rotor. Assuming that the three blades contributed equally to the thrust and gave rise to an effective axial force acting at the location of $x/R = 0.63$ along the span from the rotor axis (which was previously deduced by Ref. [16] in which measurements of the axial thrust on the shaft were compared with the out-of-plane bending

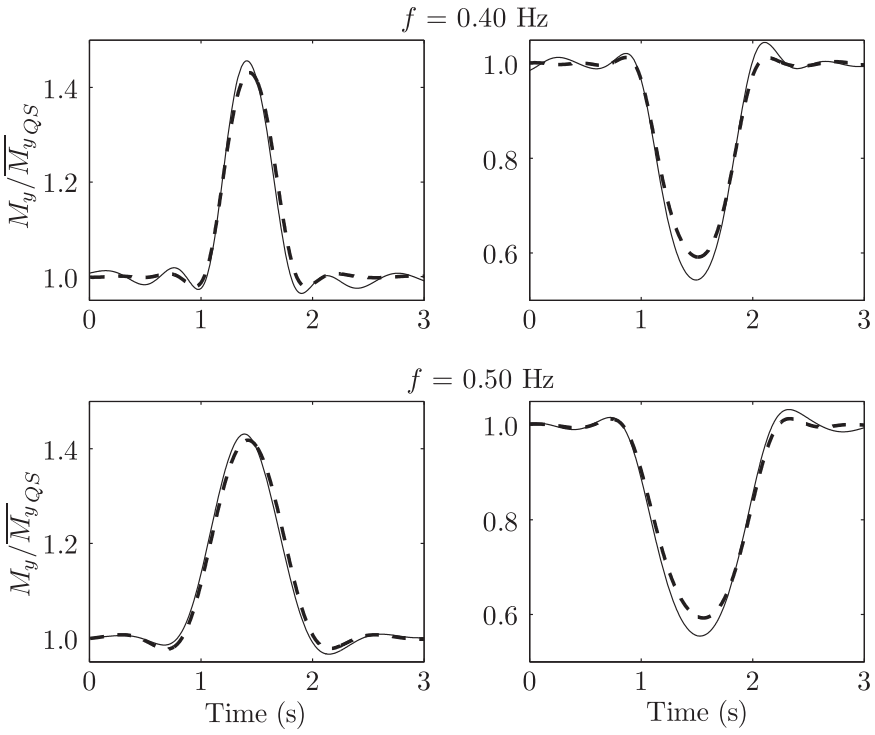

Fig. 16. Time histories of the out-of-plane bending moment response for a discrete half-sinusoidal perturbation (both positive and negative), for the frequencies $f = 0.40$ and 0.50 Hz and Current number of $\mu = 0.250$. A reconstruction based on the steady forcing is depicted by the dashed curve.

moment), a coefficient of $C_l = 0.03$ is predicted from the responses at the lowest frequency in this present study. Therefore, the value of the coefficient is within the bounds that was estimated by Ref. [23]. This is despite the discrepancies between the experimental set-ups and the control strategies in the different sets of experiments between the present study and those by Ref. [23].

The present study also provides a useful set of blade load responses to validate numerical models. Relatively low fidelity dynamic inflow models, based on a pseudo added mass have been adopted in simulation codes for tidal turbines [4]. However, these were adapted from helicopter rotors and have not been rigorously validated for tidal turbines. It would also be useful to compare the

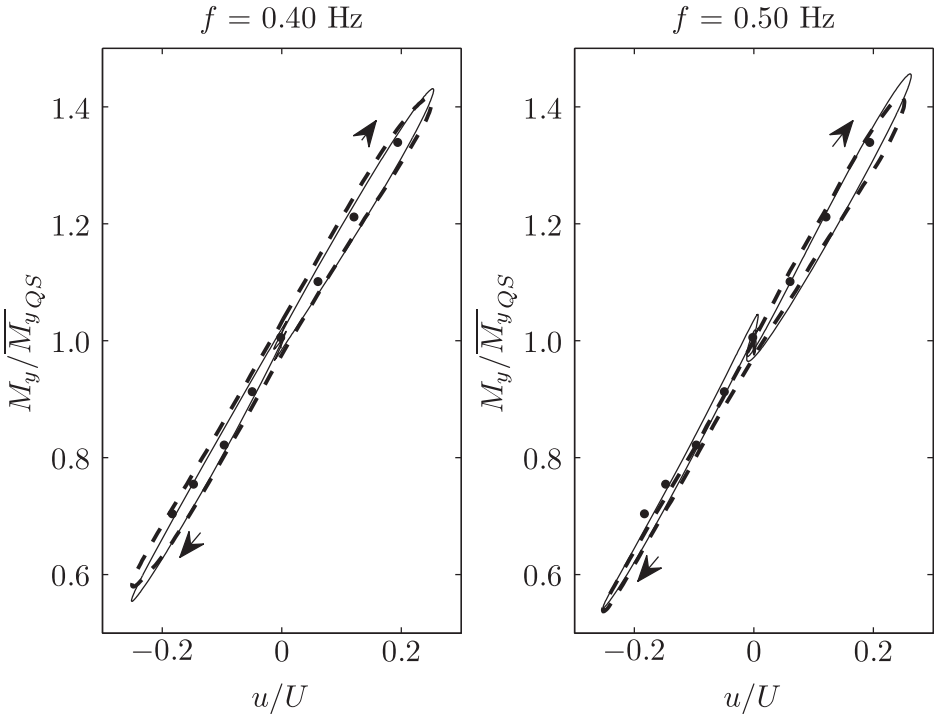

Fig. 17. Hysteresis loops of the out-of-plane bending moment response for a discrete half-sinusoidal perturbation (both positive and negative), for the frequencies $f = 0.40$ and 0.50 Hz and Current number of $\mu = 0.250$. The response to the single frequency oscillatory forcing at the equivalent frequency and Current number is superimposed as the dashed curve.

results with more complex vortex wake-based models; see Ref. [11]. These models could assist with understanding the nature of the hydrodynamic circulatory phenomena which is believe effectively reduce the axial added inertia at higher frequencies.

The ability to predict the amplitudes of the multi-frequency forcing and the general response of a discrete half-sinusoidal perturbations is significant. It implies that it could offer blade designers a relatively simple technique to obtain the fatigue loading from a turbulence spectrum and a reliable estimate of the response to large, coherent eddies. The study has also emphasised that the single frequency response offers an inherently better prediction of the unsteady response than could be achieved by using only the steady loading. The ability to recover the amplitudes of a multi-frequency forcing is also an interesting finding. It suggests that reliable estimates of the single amplitudes (that are required to develop the amplitude part of the transfer function) could be obtained by performing a limited series of multi-frequency tests. As conducting experiments are expensive and time-consuming, test programmes could be shorter in duration or more tests could be completed within a fixed time frame.

It is also important to consider that the phase is typically ignored in a stochastic modelling approach, as its effects are assumed to be able to be averaged out. These findings demonstrate that for a tidal turbine, the phase contribution is not only present but can be of greater magnitude than observed for single frequency cases. Whilst the magnitude of the inertia component is relatively small compared to the total load, as previously stated, it is important to consider that the fluid and structural inertias are expected to be of the same order of magnitude [23]. Therefore, the added inertia may also have significant implications for control purposes as well as for fatigue loads.

9. Conclusions

This study quantified the relative contribution of the hydrodynamic unsteadiness to the blade-root bending moments on tidal turbines, which has previously not been established. For single frequency oscillations about an operating state where the boundary layer is believed to remain primarily attached across the outer span sections, the unsteady blade loads increase with frequency and exceed the steady loads by up to 15%.

The out-of-plane bending moment also exhibits a phase-lead over the velocity forcing, which is consistent with the effects of dynamic inflow and non-circulatory forcing. The total hydrodynamic bending moment in-phase with acceleration was approximately a factor of 2.7 greater than the non-circulatory contribution at relatively low frequencies. However, it decreases with frequency, and circulatory effects act in opposition to the non-circulatory forcing at high frequencies.

The amplitudes of multi-frequency responses can be reconstructed using a superposition of the amplitudes and phases of the constituent single frequency oscillatory loading. The oscillatory response can also be applied to model the response to a large eddy passing over the rotor. Therefore, blade designers could potentially use the single frequency response to synthesise the unsteady load amplitudes from a turbulence spectrum. It also implies that a blade designer could obtain the amplitude part of the transfer function efficiently from a limited series of multi-frequency tests.

Importantly, for multi-frequency responses that comprise relatively high frequencies, the phase is under-predicted using a superposition of the single frequency response. Therefore, not only can the phase not be averaged out in a stochastic model, it is larger than would be predicted using a single frequency response. This is significant as the fluid to structural inertias is of the same magnitude.

Acknowledgements

This research was conducted as part of a Ph.D. programme undertaken by I. A. Milne and funded by the New Zealand Bright Futures Top Achiever Doctoral Scholarship. The experimental equipment was built with the support of the UK EPSRC grant EP/F062036/1 “Feasibility of an Innovative Methodology for Testing Marine Current Turbines in Unsteady Flow”. The authors wish to also acknowledge the Department of Naval Architecture and Marine Engineering at the University of Strathclyde for technical expertise and support.

References

[1] Anyi M, Kirke B, Ali S. Remote community electrification in Sarawak, Malaysia. Renew Energy 2010;35:1609–13.
[2] Bahaj AS, Molland AF, Chaplin JR, Batten WMJ. Power and thrust measurements of marine current turbines under various hydrodynamic flow conditions in a cavitation tunnel and a towing tank. Renew Energy 2007;32:407–26.
[3] Barltrop N, Varyani KS, Grant A, Clelland D, Xuan P. Wave-current interactions in marine current turbines. Proc Inst Mech Eng – Part M – J Eng Marit Environ 2006;220:195–203.
[4] Bossanyi E. GH Tidal Bladed theory manual. Bristol, UK: Garrad Hassan and Partners; 2009.
[5] Burton T, Sharpe D, Jenkins N, Bossanyi E. Wind energy handbook. John Wiley and Sons; 2001.
[6] Coleman HW, Steele WG. Experimental validation, and uncertainty analysis for engineers. 3rd ed. John Wiley and Sons; 2009.
[7] Fraenkel P. Marine current turbines: pioneering the development of marine kinetic energy converters. Proc Inst Mech Eng Part A: J Power Energy 2007;221:159–69.
[8] Galloway PW, Myers LE, Bahaj AS. Studies of a scale tidal turbine in close proximity to waves. In: Proceedings of the 3rd International Conference on Ocean Energy, Bilbao, Spain; 2010.
[9] GL. Rules for classification and construction, IV industrial services, part 14 offshore wind energy, guideline for the certification of ocean energy converters part 1 ocean current turbines. 2005.
[10] Khan MJ, Bhuyan G, Iqbal MT, Quaicoe JE. Hydrokinetic energy conversion systems and assessment of horizontal and vertical axis turbines for river and tidal applications: a technology status review. Appl Energy 2009;86:1823–35.
[11] Leishman JG. Challenges in modelling the unsteady aerodynamics of wind turbines. Wind Energy 2002;5:85–132.
[12] Leishman JG. Principles of helicopter aerodynamics. 2nd ed. Cambridge Aerospace: Cambridge University Press; 2006.
[13] Liu P, Veitch B. Design and optimization for strength and integrity of tidal turbine rotor blades. Energy 2012;46:393–404.
[14] Maganga F, Germain G, King J, Pinon G, Rivoalen E. Experimental study to determine flow characteristic effects on marine current turbine behaviour. IET Renew Power Gener 2010;4:498–509.
[15] Milne IA. An experimental investigation of turbulence and unsteady loading on tidal turbines. Ph.D. thesis. The University of Auckland; 2014.
[16] Milne IA, Day AH, Sharma RN, Flay RGJ. Blade loads on tidal turbines in planar oscillatory flow. Ocean Eng 2013;60C:163–74.
[17] Peters DA, Boyd DD, He CJ. Finite-state induced-flow model for rotors in hover and forward flight. J Am Helicopter Soc 1989;34:5–17.
[18] Sarpkaya T, Isaacson M. Mechanics of wave forces on offshore structures, vol. 96. Van Nostrand Reinhold Company New York; 1981.
[19] Selig MS, Guglielmo JJ, Broeren AP, Gigure P. Summary of low-speed airfoil data, vol. 1. Virginia Beach, VA, USA: SoarTech Publications; 1995.
[20] Snel H, Schepers JG. Joint investigation of dynamic inflow effects and implementation of an engineering method. 1995. Technical Report ECN-94–104.
[21] Somers DM. Design and experimental results for the S814 airfoil. Subcontractor Report NREL/SR–440–6919. Pennsylvania: Airfoils Incorporated. State College; 1997.
[22] Sutherland HJ. On the fatigue analysis of wind turbines. Technical Report SAND99–0089. Sandia National Laboratories; 1999.
[23] Whelan JI. A fluid dynamic study of free-surface proximity and inertia effects of tidal turbines. Ph.D. thesis. Imperial College of Science, Technology and Medicine; 2010.
[24] Whelan JI, Graham JMR, Piero J. A free-surface and blockage correction for tidal turbines. J Fluid Mech 2009;624:281–91.
[25] Wolfram J. On assessing the reliability and availability of marine energy converters: the problems of a new technology. Proc Inst Mech Eng Part O: J Risk Reliab 2006;220:55–68.
[26] Zhou F, Mahfuz H, Alsenas GM, Hanson HP. Static and fatigue analysis of composite turbine blades under random ocean current loading. Mar Technol Soc J 2013;47:59–69.